11-2014

# Does the worsening galactic cosmic radiation environment observed by CRaTER preclude future manned deep space exploration?

Nathan A. Schwadron
*University of New Hampshire*, Nathan.Schwadron@unh.edu

J. B. Blake
*Aerospace Corporation*

Anthony Case
*Harvard Smithsonian Center for Astrophysics*

Colin J. Joyce
*University of New Hampshire*, Colin.Joyce@unh.edu

Justin Kasper
*University of Michigan - Ann Arbor*

*See next page for additional authors*



## Recommended Citation

Schwadron, N. A., et al. (2014), Does the worsening galactic cosmic radiation environment observed by CRaTER preclude future manned deep space exploration?, Space Weather, 12, 622–632, doi:10.1002/2014SW001084.

AGU PUBLICATIONS

Space Weather

RESEARCH ARTICLE

10.1002/2014SW001084

Special Section:
The Crater Special Issue of Space Weather: Building the Observational Foundation to Deduce Biological Effects of Space Radiation

Key Points:
- GCR radiation is increasingly hazardous
- Radiation limited duration for missions in deep space
- Timing during solar cycle of missions remains a critical factor

Correspondence to:
N. A. Schwadron,
n.schwadron@unh.edu

Citation:
Schwadron, N. A., et al. (2014), Does the worsening galactic cosmic radiation environment observed by CRaTER preclude future manned deep space exploration?, *Space Weather*, *12*, 622–632, doi:10.1002/2014SW001084.

Received 30 MAY 2014
Accepted 1 OCT 2014
Accepted article online 4 OCT 2014
Published online 8 NOV 2014

# Does the worsening galactic cosmic radiation environment observed by CRaTER preclude future manned deep space exploration?

**N. A. Schwadron[1], J. B. Blake[2], A. W. Case[3], C. J. Joyce[1], J. Kasper[3,4], J. Mazur[2], N. Petro[5], M. Quinn[1], J. A. Porter[6], C. W. Smith[1], S. Smith[1], H. E. Spence[1], L. W. Townsend[6], R. Turner[7], J. K. Wilson[1], and C. Zeitlin[8]**

[1]Space Science Center, University of New Hampshire, Durham, New Hampshire, USA, [2]The Aerospace Corporation, El Segundo, California, USA, [3]High Energy Astrophysics Division, Harvard-Smithsonian Center for Astrophysics, Cambridge, Massachusetts, USA, [4]Department of Atmospheric, Oceanic and Space Sciences, University of Michigan, Ann Arbor, Michigan, USA, [5]Goddard Space Flight Center, Greenbelt, Maryland, USA, [6]Department of Nuclear Engineering, University of Tennessee, Knoxville, Knoxville, Tennessee, USA, [7]Analytic Services Inc., Arlington, Virginia, USA, [8]Southwest Research Institute, Earth Oceans and Space Science, University of New Hampshire, Durham, New Hampshire, USA

**Abstract** The Sun and its solar wind are currently exhibiting extremely low densities and magnetic field strengths, representing states that have never been observed during the space age. The highly abnormal solar activity between cycles 23 and 24 has caused the longest solar minimum in over 80 years and continues into the unusually small solar maximum of cycle 24. As a result of the remarkably weak solar activity, we have also observed the highest fluxes of galactic cosmic rays in the space age and relatively small solar energetic particle events. We use observations from the Cosmic Ray Telescope for the Effects of Radiation (CRaTER) on the Lunar Reconnaissance Orbiter to examine the implications of these highly unusual solar conditions for human space exploration. We show that while these conditions are not a show stopper for long-duration missions (e.g., to the Moon, an asteroid, or Mars), galactic cosmic ray radiation remains a significant and worsening factor that limits mission durations. While solar energetic particle events in cycle 24 present some hazard, the accumulated doses for astronauts behind 10 g/cm$^2$ shielding are well below current dose limits. Galactic cosmic radiation presents a more significant challenge: the time to 3% risk of exposure-induced death (REID) in interplanetary space was less than 400 days for a 30 year old male and less than 300 days for a 30 year old female in the last cycle 23–24 minimum. The time to 3% REID is estimated to be ~20% lower in the coming cycle 24–25 minimum. If the heliospheric magnetic field continues to weaken over time, as is likely, then allowable mission durations will decrease correspondingly. Thus, we estimate exposures in extreme solar minimum conditions and the corresponding effects on allowable durations.

## 1. Introduction

Ionizing radiation from galactic cosmic rays (GCRs) and solar energetic particles (SEPs) remains a significant challenge to long-duration crewed missions to deep space. Human beings face a variety of consequences ranging from acute effects (radiation sickness) to long-term effects including cancer induction [cf. *NRC*, 2008] and damage to organs including the heart and brain. The risk is a function of the effective dose, which is related both to energy per unit mass (expressed in Gy = J/kg) absorbed by tissue organs, and the biological effectiveness of the radiation. In this paper, we use recent measurements from the Cosmic Ray Telescope for the Effects of Radiation (CRaTER) [*Spence et al.*, 2010] zenith-facing D1/D2 detectors to determine dose and dose equivalent rates (http://prediccs.sr.unh.edu/craterweb) on the Lunar Reconnaissance Orbiter (LRO). We also utilize measurements from the CRIS instrument [*Stone et al.*, 1998] aboard the ACE spacecraft to accurately quantify the levels of radiation exposure. We assume representative areal densities of 0.3 g/cm$^2$, 10 g/cm$^2$ aluminum (Al), and 20 g/cm$^2$ shielding, corresponding to thin, intermediate, and nominal spacecraft shielding, respectively. We detail lens, organ dose equivalents, and effective dose as a function of time based largely on CRaTER observations and modeling.

Effective dose (expressed in Sv, the weighted equivalent of a joule of radiation energy absorbed in a kilogram of tissue) is used to quantify the effect of radiation on the human body. It is determined using tissue

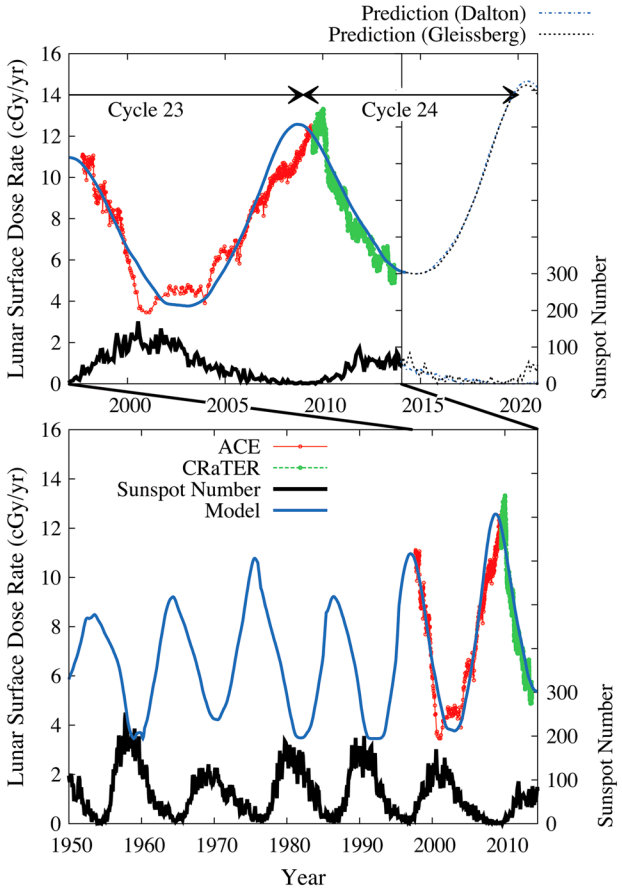


**Figure 1.** Evolving and increasingly hazardous radiation levels in space. (top) ACE dose rates (red) are based on fits to CRIS spectra [*O'Neill*, 2006]; CRaTER measurements (green) from the zenith-facing D1/D2 detectors are used as proxies for lens dose rates behind 0.3 g/cm$^2$ Al shielding *Schwadron et al.* [2012]. The sunspot number predictions (the lower black and blue dashed lines) show two cases based on a Gleissberg-like and a Dalton-like minimum, the results of which are similar. The dose predictions (solid blue line and the upper black and blue dashed lines) are from a sunspot-based model of the heliospheric magnetic field and the correlated variation in modulation of GCRs (Appendix A). The ACE data, CRaTER data, and model results are projected to the lunar surface. (bottom) Same as Figure 1 (top) but for a longer time span.

weighting factors involving organ dose equivalents, which quantify the cancer risk induced by different types of radiation. The risk of exposure-induced death (REID) quantifies the risk (at the 95% confidence level) of an exposed individual dying from a certain cancer as a function of the effective dose. NASA has established career cancer risk limits [*NASA*, 2007] which specify that the risk should be limited to no more than a 3% REID at a 95% confidence level using a statistical approach to account for uncertainties [*NRC*, 2012]. The career effective dose before the 3% REID limit is reached is 0.47 Sv for a 30 year old female and 0.62 Sv for a 30 year old male [*NRC*, 2008]. For reference, the American Cancer Society reported that 23% of all deaths in 2004 were due to cancer [*ACS*, 2007]. Thus, with current limits, the effective dose received in space adds an additional increment of up to 3% to this risk. Other potentially serious health risks are not accounted for in this methodology.

The deep solar minimum between cycles 23 and 24 and the activity in cycle 24 differed significantly from those of the prior cycle [*Schwadron et al.*, 2011; *McComas et al.*, 2013; *Schwadron et al.*, 2014]. During this period, the fast solar wind was slightly slower, was significantly less dense and cooler, had lower mass and momentum fluxes [*McComas et al.*, 2008], and weaker heliospheric magnetic fields [*Smith and Balogh*, 2008] compared to earlier cycles. During the rise of activity in cycle 24 the mass flux of solar wind remained low [*McComas et al.*, 2013] and the magnetic flux of the heliosphere remained at significantly lower levels than observed at previous solar maxima in the space age [*Smith et al.*, 2013]. Cycle 24 is the weakest solar maximum of the space age, which continues the highly anomalous trends observed in the deep cycle 23–24 minimum. Conditions during the cycle 23–24 minimum appear to be similar to conditions at the beginning of the 1800s at the start of the Dalton Minimum [*Goelzer et al.*, 2013]. Taken together, these recent changes suggest that the next solar minimum may continue to show declining sunspot numbers, associated with declining values of magnetic flux and further reductions in solar wind particle flux.

The anomalously weak heliospheric magnetic field and low solar wind flux during the last solar minimum have resulted in GCRs achieving the highest flux levels of the space age [*Mewaldt et al.*, 2010], and fluxes continue to be unusually elevated through the cycle 24 maximum. It is unknown if the recent anomalous deep solar minimum is a harbinger of larger changes in the near future or if the unusual changes in GCR fluxes and conditions on the Sun have an impact on Earth's atmosphere. Figure 1 illustrates the critical growing record of the dose rate throughout the Advanced Composition Explorer (ACE) and LRO missions that quantifies the changing conditions and radiation hazards posed by GCRs.

## 2. Worsening Hazard From Galactic Radiation

The measurements of ACE in Figure 1 result from fitting heavy ion distributions measured by ACE/CRIS [*Stone et al.*, 1998] to a model [*O'Neill*, 2006] for GCR distributions, which are then fed in to High-charge (Z) and Energy (HZE) Transport (HZETRN) 2005 to estimate associated dose rate (see also Appendix B). These ACE data are provided up to 2010. After 2010, we use direct measurements from CRaTER for the dose rate.

The model, for which results are shown in Figure 1 (blue curves), is developed in Appendix A and utilizes sunspot number to estimate the magnetic flux of the heliosphere [*Goelzer et al.*, 2013]. In this model, sunspot numbers serve as a proxy for solar activity and the frequency of coronal mass ejections (CMEs). CME ejection causes the buildup of magnetic flux in the heliosphere. *Goelzer et al.* [2013] reconcile in situ measurements over the past 40 years and show general agreement with magnetic field reconstructions using paleogenic $^{10}$Be data. The results suggest that the protracted cycle 23 with an extended period of low solar activity sustained disconnection of magnetic flux without the increased reinjection of new magnetic flux from CMEs. This led to the cycle 23 decay of heliospheric magnetic flux, which helps explain why the heliospheric magnetic field intensity dropped to the lowest levels in the space age.

Our model for dose rates uses the magnetic field model of *Goelzer et al.* [2013] to deduce the modulation potential of GCRs [e.g., *O'Neill*, 2006; *Badhwar and O'Neill*, 1994]. The modulation potential allows specification of distribution functions across a range of species with differing numbers of nucleons $A$ and charge state $Z$. *Schwadron et al.* [2012] demonstrated that the modulation potential can be understood based on the slab turbulence model of cosmic ray diffusion [*le Roux et al.*, 1999]. The results of Appendix A confirm the basic correlation between the modulation potential and magnetic field strength as predicted from theory. Using the modulation potential with the HZETRN model, we then determine GCR-associated dose rates. The resulting model is used to extrapolate back in time through the space age and to project beyond the current date using a sunspot-based reconstruction of the heliospheric magnetic field [*Smith et al.*, 2013; *Goelzer et al.*, 2013].

The HZETRN code transports the incident charged ions and their nuclear reaction secondary particles (protons, neutrons, deuterons, tritons, 3He, 4He, and heavier ions) generated from nuclear collisions. Pions were not produced or transported in these runs. The code outputs, selectable by the user, include particle fluences, dose, dose equivalent, effective dose, and linear energy transfer (LET) distributions. For the HZETRN model results, we use effective dose and organ doses for the assumed aluminum shield configurations. Organ doses ($D$) are in units of centigray (cGy) where 1 cGy = 1 rad and 100 cGy = Gy = 1 J/kg. Organ dose equivalents ($H$), which are the product of dose with a quality factor, $Q$ ($H = Q \times D$), are in centisievert (cSv) where 1 cSv = 1 rem and 100 cSv = 1 Sv = 1 J/kg. The units of effective dose ($E$) are also cSv. The HZETRN effective dose is calculated from

$$E = \sum_T w_T H_T \tag{1}$$

where $H_T$ is the organ dose equivalent for the organ specified by $T$ (e.g., skin, eye, lens, etc.). The tissue (organ) weighting factors $w_T$ are the proportionate detriment of the organ when the whole body is irradiated and are tabulated in Table 5.1 of *National Council on Radiation Protection and Measurements* (*NCRP*) [1993].

The slowing activity in solar cycle 23 has led to a depletion of heliospheric magnetic flux [*Connick et al.*, 2009], which weakens the modulation of GCRs and leads to higher GCR fluxes. The dose rates observed in Figure 1 are therefore higher during the 2008–2009 lull in solar activity as compared to the deep solar minimum near 1997. The mini-maximum in cycle 24 is consistent with a continued decline in solar activity relative to previous maxima of the space age.

The trends in weakening solar activity are extremely consistent with the beginning of a period from 1790 to 1830 called the Dalton grand minimum [*Goelzer et al.*, 2013] or alternatively the less extreme Gleissberg minimum in the period 1890–1920 [*Smith et al.*, 2014]. Specifically, in the case of the Dalton minimum, the typicalž solar maximum from 1785 to 1790 resembles the more modern maximum from 1998 to 2003. When we compare the unusually low sunspot numbers of the maxima for 1804 and 2013, we find that both are uncommonly low for maxima throughout the space age. In the case of the Gleissberg minimum, the solar maximum of 1870 was marginally higher than the maximum of 2001 while the maximum of 1883 is also slightly higher than the maximum of 2013. Solar activity over the next ~ 5 years (through 2020) was

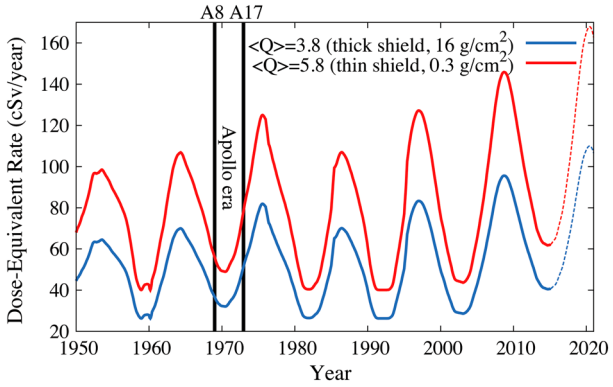


**Figure 2.** Dose equivalent rates in interplanetary space shown for different average quality factors: $\langle Q \rangle = 5.8$, measured by CRaTER behind thin shielding and $\langle Q \rangle = 3.8$ measured by RAD behind thicker shielding. Black lines indicate times spanned by the Apollo missions from Apollo 8 (A8) to 17 (A17).

estimated along with the weakening magnetic field [*Goelzer et al.*, 2013; *Smith et al.*, 2014] based on the historic behavior in sunspot evolution in the period from 1804 to 1810 for the Dalton-like grand minimum and in the period from 1883 to 1889 for the Gleissberg-like minimum. Applying the modulation model (Appendix A), we estimate the evolution of dose rates (Figure 1). We note that the peak dose rate between cycles 23 and 24 agrees well with the estimate reported recently by *Spence et al.* [2013], which includes contributions of lunar albedo, of 13.6 cGy/yr. The predictions for both the case of a Gleissberg-like and Dalton-like minimum are quite similar. While these are only estimates, it is clear that the declining solar activity observed in cycle 23 is presently causing elevated dose rates and a more dangerous space environment.

There are two major considerations needed to translate CRaTER-measured doses to dose equivalents. The first consideration is the extrapolation from the thin shielding ($\sim 0.3$ g/cm$^2$ Al) on CRaTER to the thicker shielding ($\sim 16$ g/cm$^2$) on typical spacecraft. The shielding extrapolation is done using the High-charge (Z) and Energy Transport code (HZETRN) as detailed in the supporting information (Appendix B). The second consideration is the conversion from dose to dose equivalent using linear energy transfer (LET) spectra. We estimate the dose equivalent using the observed LET spectra by LRO/CRaTER [*Case et al.*, 2013] in its almost unshielded zenith-facing detectors (D1/D2) and by Mars Science Laboratory/Radiation Assessment Detector (MSL/RAD) during the MSL cruise to Mars [*Zeitlin et al.*, 2013], in addition to using results from models. In the case of CRaTER and RAD, we first convert the measured LET spectrum in Si to the LET spectrum in water [*Benton et al.*, 2010]. We then integrate across the LET spectrum multiplied by the quality factor [*ICRP*, 1991], which is a function of LET in water. One way to quantify the difference between dose ($D$) and dose equivalent ($H$) is the average quality factor, $\langle Q \rangle = H/D$. For CRaTER, we find $\langle Q \rangle \sim 5.8$, whereas RAD shows a lower average quality factor $\langle Q \rangle \sim 3.8$. This lower quality factor on RAD is due to much thicker shielding ($\sim 16$ g/cm$^2$ Al shielding for RAD as compared to $\sim 0.2$ g/cm$^2$ for CRaTER). Quality factors of $\sim$3–4 are quite typical of results of models such as HZETRN when moderate shielding is present [e.g., *Zeitlin et al.*, 2013; *Schwadron et al.*, 2010a, Appendix B]. Results for dose equivalent rates are shown in Figure 2. Notably, results show the significant increase in dose equivalent rates in subsequent solar minima after the mid-1990s. In each subsequent solar minimum, we observe an $\sim 20\%$ increase in the dose equivalent rate.

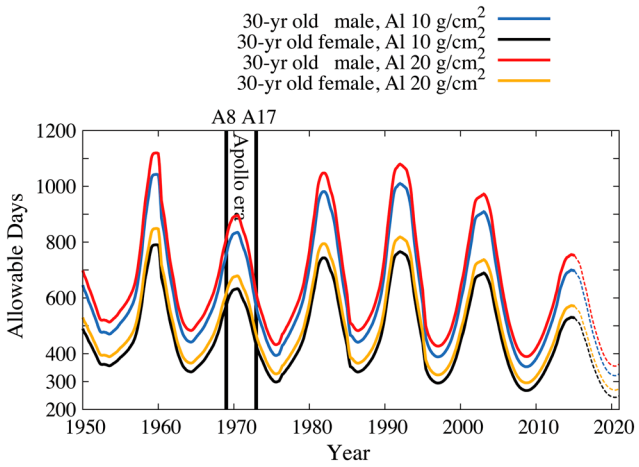


**Figure 3.** Days in interplanetary space before a 30 year old astronaut reaches their career radiation limit for 3% risk of exposure-induced death (REID) at the 95% confidence level. Shown are maximum days before 3% REID limits are reached assuming different amounts of Al shielding (10 g/cm$^2$ and 20 g/cm$^2$). Black lines indicate times spanned by the Apollo missions from Apollo 8 (A8) to Apollo 17 (A17).

As a practical exercise, we compute the length of time within acceptable risk that an astronaut could be exposed to the level of GCR radiation shown in Figure 1. Model differences in susceptibility to cancer, body mass,

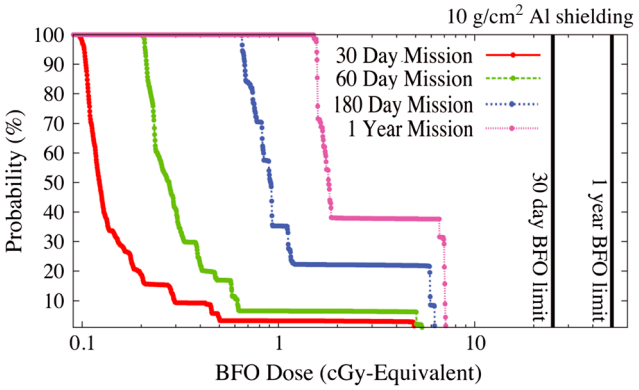


**Figure 4.** Probability (%) versus integrated BFO dose for 30 day to 1 year missions. We use the PREDICCS database [*Schwadron*, 2012] (http://prediccs.sr.unh.edu) to build up statistics for the probability of SEP events of varying integrated dose behind spacecraft shielding (10 g/cm$^2$). The database currently provides doses for the period from July 2011 through April 2014. The PREDICCS doses are derived from proton spectra and use dose in 10 g/cm$^2$ water as a proxy for the blood forming organ (BFO) dose.

and self-shielding lead to different effective dose limits for males and females and correspond to the same risk (3% REID at 95% confidence). For example, a 30 year old male astronaut has an effective dose limit of 62 cSv, which is larger than the limit of 47 cSv for a 30 year old female [*NRC*, 2008]. These limits increase with age. For example, the limit is 95 cSv for a 45 year old male. These limits are used to estimate the number of days in deep space before an astronaut reaches the 3% REID limit (see Figure 3), where the number of allowable days in interplanetary space is given by the effective dose limit divided by the effective dose rate from the HZETRN model. We have included estimates using both 10 g/cm$^2$ and 20 g/cm$^2$ Al shielding. It is apparent that the maximum number of days in interplanetary space below the 3% REID limit is decreasing substantially (by $\sim$ 20%) in each successive solar minima beyond the mid-1990s. In the 2020 minimum, for example, the limiting allowable time for a 30 year old male and female in deep space is less than or similar to 1 year.

Figures 1–3 show that the doses from GCRs are far smaller during solar maximum when elevated magnetic field intensities in the heliosphere help shield the inner heliosphere from GCRs. However, during solar maximum the more frequent events from solar energetic particles (SEPs) elevate the radiation hazard. (Note that SEP events are often characterized as solar proton events, SPEs, which emphasize observed elevated proton fluences.) We study the probability of SEP events using a near-real-time tool called PREDICCS (Predictions of Radiation from REleASE, EMMREM, and Data Incorporating the CRaTER, COSTEP, and other SEP measurements, http://prediccs.sr.unh.edu [*Schwadron*, 2012]), an online system for nowcasting the radiation environment in near-Earth, lunar, and Martian space environments. The PREDICCS tool has been shown to be very accurate for dose rate calculations [*Joyce et al.*, 2013] in comparison to CRaTER observations. We use the tool here to determine the probability distribution of integrated doses of SEP events from mid-2011 through April 2014, which covers the progression in the rise of solar activity in cycle 24.

Figure 4 shows the probability of an integrated blood forming organ (BFO) dose for a 30 day, 60 day, 180 day, and 1 year mission assuming 10 g/cm$^2$ Al shielding. The 30 day BFO dose limit is 25 cGy equivalent, and the 1 year limit is 50 cGy equivalent [*NRC*, 2008]. Note that instead of cSv, we use units of cGy equivalent to characterize the biological efficiency for noncancer effects. Specifically, the dose (in cGy equivalent) is given by $D(\text{cGy eq}) = D(\text{cGy}) \times \text{RBE}$ where RBE (relative biological effectiveness) quantifies radiation effects in humans [*National Council on Radiation Protection and Measurements (NCRP)*, 2000]. For SPE protons we use an RBE value of 1.5. The probability distribution in Figure 4 represents a limited sample during the current phase of solar activity, and it is unclear how this might change in the future. Singular large events contribute substantially to the net integrated dose. As such, any interplanetary flight requires a storm shelter inside the spacecraft of at least 20 g/cm$^2$ to prevent excessive exposure from SPEs. Because of the small cycle 24, it is important to supplement the probability distribution determined here with additional measurements as they become available. At the very least, this highlights the need for an increased baseline of radiation measurements from instruments like CRaTER and RAD.

While conditions during cycle 24 suggest low probabilities for an extreme event at the limit of acceptable risk, questions to consider when including SEP contributions are (1) whether current conditions will continue to prevail and (2) if large events should be considered separately when estimating risk. Given the opportunity to reduce SEP dose with adequate warning and access to a storm shelter, the exposure is likely dominated by GCR, which is not significantly attenuated by shielding.

## 3. Summary

The results of this analysis show that declining solar activity and the subsequently weakening heliospheric magnetic field in the protracted solar cycle 23–24 minimum leads to an increasingly hazardous radiation environment due to elevated fluxes of galactic cosmic rays. We project out to the cycle 24–25 solar minimum and find an elevated dose equivalent rate of ~0.3 cSv/d in interplanetary space behind 16 g/cm$^2$ nominal spacecraft shielding or equivalently ~ 0.15 cSv/d on the lunar surface where roughly half of the incident radiation is blocked by the Moon [*Spence et al.*, 2013]. The estimate for interplanetary space is in reasonable agreement with a previous estimate made for similar shielding by *Mewaldt et al.* [2005].

Notably, the average 1 year travel time between Earth and Mars (6 months for travel to and return from Mars) is comparable to the time to 3% REID during solar minimum for a 30 year old astronaut, for GCR exposure alone (i.e., no contribution from SEP events). The time to 3% REID was less than 400 days for a 30 year old male and less than 300 days for a 30 year old female in the last cycle 23–24 minimum. The time to 3% REID is estimated to be ~ 20% lower in the coming cycle 24–25 minimum.

Exploration missions near solar maximum may be preferable in order to limit the galactic cosmic ray radiation hazard. Further, the radiation hazard due to solar energetic particles is lessened in the mini solar cycle 24 due to unusually low levels of solar activity compared to previous solar maxima. Total integrated doses behind a nominally shielded spacecraft are far less than worst-case scenarios (~ 1 Sv integrated dose equivalent). Additionally, in cases of extreme SEP events, astronauts would position themselves behind thicker shielding (>20 g/cm$^2$ Al) to reduce the SEP radiation risk even further [*Cucinotta et al.*, 2013].

Currently, our sample of solar energetic particle events measured directly over the course of a solar cycle remains limited, and the actual probability of extreme events remains poorly understood. This highlights the importance of acquiring better statistical information on solar energetic particle events using an increasing baseline of direct observations (e.g., LRO/CRaTER and MSL/Rad).

In conclusion, our analysis shows that if the heliospheric magnetic field continues to weaken over time, as is likely, then allowable mission durations will decrease correspondingly. Our estimates of exposures in an extreme solar minimum demonstrate its significance for long-term human exploration missions.

## Appendix A: Modulation of Galactic Cosmic Rays: The Solar Modulation Potential

Modulation of GCRs has caused the dose rates measured by CRaTER to trend lower throughout the course of the LRO mission to date. Observations of GCR dose rates, interplanetary magnetic field strengths, and current sheet tilt angle [*Schwadron et al.*, 2012] provide context for the effects of modulation. Jumps in magnetic field strength observed appear to be consistent with sharp decreases observed in dose. Step-like features have been analyzed in detail [*Case*, 2011]. The enhancements in the heliospheric magnetic field strength are due to closed magnetic flux fed into the heliosphere by coronal mass ejections (CMEs) [*Owens and Crooker*, 2006; *Owens et al.*, 2007; *Schwadron et al.*, 2008, 2010b], which leads to increased modulation [e.g., *Newkirk et al.*, 1981; *Cliver and Ling*, 2011]. Therefore, the reductions in GCR flux as solar activity increases are likely caused in part by increased interplanetary magnetic field strength associated with increased rates of CMEs.

The structure of the heliospheric magnetic field also changes over the solar cycle. Near solar minimum, regions of uniform polarity emanate from the poles of the Sun. As activity increases, the solar magnetic field becomes increasingly disordered and sources of magnetic flux migrate from the poles into the equatorial regions. Eventually, as the Sun evolves through solar maximum, magnetic flux migrates through the equatorial region and the polarity of the heliospheric magnetic field reverses [*Owens et al.*, 2007; *Schwadron et al.*, 2008]. Then as the Sun declines into the next solar minimum configuration, the reversed polarity fields coalesce into polar coronal holes and the heliospheric magnetic field again attains an ordered structure. This heliospheric magnetic field reversal process is likely driven through interchange reconnection between open magnetic flux and coronal mass ejections [*Crooker et al.*, 2002].

*Goelzer et al.* [2013] utilize a model for the evolution of heliospheric magnetic flux where sunspot numbers serve as a proxy for solar activity and the frequency of CME ejection. CME ejection leads to the buildup of

magnetic flux in the heliosphere. The magnetic field model [*Schwadron et al.*, 2010b] takes into account (1) the conversion of magnetic flux from that introduced by CME ejection into magnetic flux open to the heliosphere and the steady solar wind from coronal holes and (2) the loss of magnetic flux through disconnection. *Goelzer et al.* [2013] reconcile in situ measurements over the past 40 years and show general agreement with magnetic field reconstructions using paleogenic $^{10}$Be data. The results suggest that the protracted cycle 23 with an extended period of low solar activity sustained disconnection of magnetic flux without the increased reinjection of new magnetic flux from CMEs. This led to the cycle 23 decay of heliospheric magnetic flux, which helps explain why the heliospheric magnetic field intensity dropped to the lowest levels in the space age.

One parameter used to track the solar magnetic reversal process is the average tilt of the heliospheric current sheet (HCS). The HCS tilt angle also correlates with the relative magnitudes of drifts experienced by cosmic rays. Near solar minimum, the heliospheric current sheet is tilted only slightly from the equatorial plane, and the relatively ordered fields of the heliosphere cause strong cosmic ray drifts. However, nearer solar maximum these cosmic ray drift patterns break down [*Fisk and Schwadron*, 1995] as the current sheet becomes strongly tilted on average and the field becomes highly disordered [*Schwadron et al.*, 2012].

The development of the solar modulation potential reduces the complexity of solving for the distribution function of galactic cosmic rays *Gleeson and Axford* [1968]:

$$f(\mathbf{r}, E, t) = f(\infty, T + \Phi) \tag{A1}$$

where $f(\mathbf{r}, E, t)$ is the distribution function of cosmic rays at position $\mathbf{r}$, total energy $E$, and time $t$. The local distribution function is related in (A1) to the distribution function beyond the modulation boundary, $f(\infty, E + \Phi)$. The total energy has the standard definition, with particle momentum $p$ given by

$$(pc)^2 = E^2 - E_0^2 \tag{A2}$$

and $E_0$ being the rest energy ($E_0 = Am_pc^2$). Therefore, $\Phi$ is the potential energy or energy loss experienced for a cosmic ray coming in from infinity.

The modulation potential is an extremely convenient tool as it allows specification of distributions across a range of species with differing numbers of nucleons $A$ and charge state $Z$. The modulation potential has been used widely in determining radiation dose from GCRs [e.g., *O'Neill*, 2006; *Badhwar and O'Neill*, 1994]. The modulation potential is often related to a dimensionless function $\phi(r)$, where

$$\Phi = |Ze|\phi(r) \tag{A3}$$

and

$$\phi(r) = \int_r^{R_b} \mathrm{d}x \frac{V(x)}{3\kappa_1(x)} \tag{A4}$$

where $r$ is heliocentric radial distance, $R_b$ is the modulation boundary, $V(x)$ is the average solar wind speed, and $\kappa_1(x)$ is related to the radial diffusion coefficient, $\kappa$. The form for $\kappa$ is based on a fit to the observed spectrum over time and species [*O'Neill*, 2006]:

$$\kappa = \kappa_1(r)P\beta \tag{A5}$$

where $P = pc/q$ is rigidity and $\beta = v/c$ where $v$ is particle speed.

*Schwadron et al.* [2012] demonstrated that the modulation potential can be understood based on the slab turbulence model of cosmic ray diffusion [*le Roux et al.*, 1999] where the parallel diffusion coefficient $\kappa_{\|} \propto r_g^2/F^2$, where the gyroradius is $r_g = pc/(qB)$ and $F = \delta B/B$ is the normalized (slab) component of heliospheric magnetic field fluctuations. The radial diffusion coefficient is $\kappa = (B_r^2/B^2)\kappa_{\|}$, where $B_r$ is the radial magnetic field strength. If $F$ is roughly constant, then the radial diffusion coefficient is proportional to the inverse square of the heliospheric field strength, $\kappa \propto B^{-2}$, and the modulation potential is proportional to the square of the magnetic field strength, $\Phi \propto B^2$. *Schwadron et al.* [2012] studied the correlation between the heliospheric magnetic field strength and the modulation and derived a power law behavior

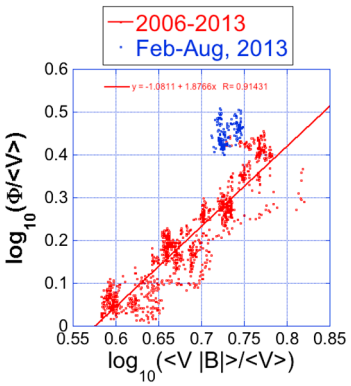


**Figure A1.** The correlation between modulation potential and heliospheric magnetic field strength provides a natural way to predict how the modulation potential will vary. We have used the modulation potential determined using ACE measurements [*O'Neill*, 2006] and the modulation potential from CRaTER measurements [*Joyce et al.*, 2014]. Hourly OMNI data (http://omniweb.gsfc.nasa.gov) were used to derive 6 month averages of solar wind speed $\langle V \rangle$ and solar wind speed times the heliospheric magnetic field strength $\langle V|B| \rangle$. The data points show the results in terms of $\log_{10}(\Phi/\langle V \rangle)$ and $\log_{10}(\langle V|B| \rangle/\langle V \rangle)$. The inferred correlation shows that $\Phi \propto |B|^{\gamma}$ where $\gamma = 1.87$, the same scaling derived by *Schwadron et al.* [2012]. Data are shown from 2006 to 2013 (red) and close to solar maximum (February–August 2013; blue). The departure from the nominal scaling with $\gamma = 1.87$ results from the formation of globally merged interaction regions (GMIRs) that enhance modulation.

$\Phi \propto |B|^{\gamma}$ where $\gamma = 1.87$. This correlation is remarkably close to the quadratic behavior predicted by the slab turbulence model [*le Roux et al.*, 1999].

The apparently simple behavior of modulation potential as a function of heliospheric magnetic field strength suggests an elegant approach to understanding the time evolution of modulation where the modulation potential utilizes the correlation function derived here

$$\Phi = \Phi_1 (V/V_1)(|B|/B_1)^{\gamma}, \tag{A6}$$

$V_1 = 400$ km/s is a reference solar wind speed, $B_1 = 1$ nT is a reference magnetic field strength, and $\Phi_1 = 33.2$ MV is a reference modulation potential. We vary the Carrington-averaged solar wind speeds based on observations through the solar cycle. These average solar wind speeds vary from 370 km/s to 430 km/s.

Another significant factor in the correlation function (A6) is the magnetic field strength that is used in the correlation. We use the results of *Goelzer et al.* [2013] for the magnetic field strength. When compared with Omni2 data, this heliospheric magnetic field model gives extremely good agreement for the total magnetic field strength [*Goelzer et al.*, 2013]. Generally, the correlation between the modulation potential and the magnetic field strength shown in Figure A1 confirms the result in equation (A6).

The departure from the almost quadratic correlation function between the modulation potential and the magnetic field strength observed in Figure A1 occurs during solar maximum (February–August 2013). The magnetic field observations show that there is a component in the magnetic field that is not associated with the Parker spiral. The observed heliospheric magnetic field contains azimuthal fields often associated with magnetic clouds and turbulent magnetic fluctuations, both of which are absent from the definition of Parker spiral. Therefore, as detailed by *Goelzer et al.* [2013], we fully expect that the total magnetic field intensity exceeds that of the Parker spiral component.

We are faced then with the question of whether we should use the Parker spiral component of the magnetic field or the total magnetic field intensity should be used in the correlation function (A6). The derived modulation potential and the results in Figure A1 suggest simply that the Parker spiral component applies to the correlation function near solar minimum conditions, but the total magnetic flux applies near solar maximum. The results point to a physical interpretation of the departure (blue points) observed in Figure A1. When CMEs are frequent near solar maximum, large-scale structures, often referred to as globally merged interaction regions (GMIRs), cause departures from the Parker field component and GMIRs participate significantly in the modulation of galactic cosmic rays [*McDonald and Burlaga*, 1997]. In fact, the step-like decreases observed in GCR fluxes and associated dose rates [e.g., *Case*, 2011; *Schwadron et al.*, 2012] are likely the direct result of formation of such global magnetic structures well beyond 1 AU in the phase of increasing activity.

The result is that we use only the Parker spiral component in the correlation function for the modulation function (A6) during solar minimum conditions. In solar maximum conditions we use the total magnetic field strength in the correlation function for the modulation potential. A weighting factor is used to transition from the solar minimum Parker spiral component to the total field strength used in solar maximum. The results shown in Figure 1 of the paper demonstrate good agreement between this simple model and observations.

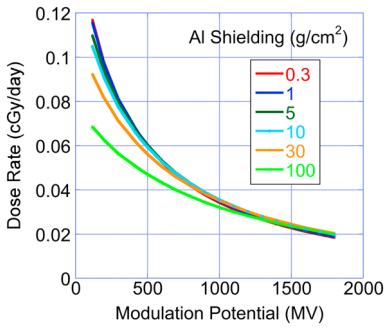


**Figure B1.** Dose rates derived from HZETRN as a function of modulation potential. Colored curves correspond to varying levels of Al shielding.

While there is good agreement between modeled and observed dose rates (Figure 1, main paper), the agreement with neutron data deduced from a similar model is less favorable [*Schwadron et al.*, 2012]. Multiple effects may contribute to the difference between the lower and higher-rigidity GCR species: (1) Deep in solar minima, three-dimensional drifts of cosmic rays become quite important [*Jokipii et al.*, 1977; *Florinski et al.*, 2003; *Potgieter and Le Roux*, 1992]. GCR protons have drift paths that differ from higher-rigidity GCRs. (2) The reduced solar wind pressure [*McComas et al.*, 2013; *Schwadron et al.*, 2014; *McComas et al.*, 2008; *Schwadron and McComas*, 2008] in the deep cycle 23–24 solar minimum has allowed the termination shock to move closer to the Sun and resulted in a weakened modulation of the heliosheath [*Scherer et al.*, 2011]. Low-rigidity GCR protons are more strongly modulated in the inner heliosheath. Therefore, higher GCR proton fluxes may penetrate the weakened heliosheath magnetic fields in the deep and extended cycle 23–24 minimum. (3) The reduction in the interplanetary magnetic field strength to the lowest values of the space age [*Goelzer et al.*, 2013; *Smith et al.*, 2013; *Connick et al.*, 2011] may preferentially enhance GCR protons. The magnitude and variance of the interplanetary magnetic field falls during solar minimum, which increases diffusion [e.g., *Wibberenz et al.*, 2002; *Manuel et al.*, 2011]. GCR protons are more sensitive to time-dependent changes in the interplanetary magnetic field strength because they have lower rigidity than heavier GCR species such as Oxygen. A sharp drop in the interplanetary magnetic field strength, like the one that occurred during the cycle 23–24 minimum, should significantly increase GCR proton fluxes while causing less pronounced increases in heavier GCRs species.

## Appendix B: Radiation Dose and Average Quality Factor Versus Shielding Thickness

The High-charge (Z) and Energy (HZE) Transport code (HZETRN) [*Wilson and Badavi*, 1986; *Wilson et al.*, 1991; *Shinn et al.*, 1991; *Cucinotta*, 1993; *Wilson et al.*, 2003; *Nealy et al.*, 2006] solves for radiation interaction with materials using a one-dimensional, analytical formulation of the Boltzmann transport equation. A three-layer version of HZETRN 2005 has been configured and implemented as a part of the Earth-Moon-Mars Radiation Environment Module, as detailed by *Schwadron et al.* [2010a] and [*Townsend et al.*, 2011]. The input into the calculations is taken from the Badhwar Neill GCR model [e.g., *O'Neill*, 2006; *Badhwar and O'Neill*, 1994] using modulation potentials ranging from 120 MV to 1800 MV in the solar cycle. This GCR model is used for space operations at the Space Radiation Analysis Group at NASA Johnson Space Center.

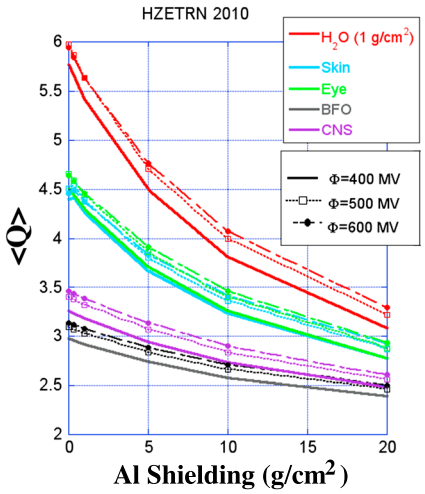


**Figure B2.** Average quality factor, $\langle Q \rangle$, derived from HZETRN 2010 [*Slaba et al.*, 2010] as a function of modulation potential, $\Phi$, shielding depth, and tissue (e.g., skin, eye, BFO, or central nervous system) or target material (e.g., $H_2O$).

Figure B1 shows results of the HZETRN model for different thicknesses of Al shielding as a function of modulation potential. For spacecraft Al shielding of ~5–10 g/cm$^2$, the dose rates are quite similar as those for the typical shielding thickness of CRaTER (~0.3 g/cm$^2$).

We have also used the 2010 version of HZETRN [*Slaba et al.*, 2010] to solve for average quality factor, $\langle Q \rangle$, as a function of Al shielding thickness (Figure B2), modulation potential, $\Phi$, and tissue or target material. The average quality factor falls with increasing Al shielding depth, consistent with the observation of a larger quality factor inferred from CRaTER for thin (~0.2 g/cm$^2$) Al shielding compared to the smaller quality factor inferred from RAD for thicker (~16 g/cm$^2$) Al shielding.

**Acknowledgments**
We thank all those who made CRaTER possible. CRaTER is primarily funded by the LRO program (contract NNG11PA03C). This work was also funded by EMMREM (grant NNX07AC14G), C-SWEPA (NASA grant NNX07AC14G), Sun-2-Ice (NSF grant AGS1135432) projects, and DoSEN (NASA grant NNX13AC89G), DREAM (NASA grant NNX10AB17A), and DREAM2 (NASA grant NNX14AG13A). CRaTER data are available at http://crater-web.sr.unh.edu.

## References

ACS (2007), *Cancer Facts and Figures 2007*, Am. Cancer Soc., Atlanta, Ga.
Badhwar, G. D., and P. M. O'Neill (1994), Long-term modulation of galactic cosmic radiation and its model for space exploration, *Adv. Space Res.*, *14*(10), 749–757.
Benton, E. R., E. V. Benton, and A. L. Frank (2010), Conversion between different forms of LET, *Radiat. Meas.*, *45*(8), 957–959, doi:10.1016/j.radmeas.2010.05.008.
Case, A. W. (2011), Galactic cosmic ray variations at the Moon, PhD thesis, Boston Univ., Boston, Mass.
Case, A. W., et al. (2013), The deep space galactic cosmic ray lineal energy spectrum at solar minimum, *Space Weather*, *11*, 361–368, doi:10.1002/swe.20051.
Cliver, E. W., and A. G. Ling (2011), The floor in the solar wind magnetic field revisited, *Sol. Phys.*, *274*, 285–301, doi:10.1007/s11207-010-9657-6.
Connick, D. E., C. W. Smith, and N. A. Schwadron (2009), The flux of open and toroidal interplanetary magnetic field as a function of heliolatitude and solar cycle, *Astrophys. J.*, *695*, 357–362, doi:10.1088/0004-637X/695/1/357.
Connick, D. E., C. W. Smith, and N. A. Schwadron (2011), Interplanetary magnetic flux depletion during protracted solar minima, *Astrophys. J.*, *727*, 8, doi:10.1088/0004-637X/727/1/8.
Crooker, N. U., J. T. Gosling, and S. W. Kahler (2002), Reducing heliospheric magnetic flux from coronal mass ejections without disconnection, *J. Geophys. Res.*, *107*, 1028, doi:10.1029/2001JA000236.
Cucinotta, F. A. (1993), Calculations of cosmic-ray helium transport in shielding materials, *Tech. Rep. NASA-TP-3354, L-17225, NAS 1.60:3354*, NASA Langley Res. Cent., Hampton, Va.
Cucinotta, F. A., L. Chappell, and M. Y. Kim (2013), Space radiation cancer risk projections and uncertainties—2012, *Tech. Rep. NASA TP 2013-217375*, NASA STI Program, Hampton, Va.
Fisk, L. A., and N. A. Schwadron (1995), The influence of intermediate-scale variations in the heliospheric magnetic field on the transport of galactic cosmic rays, *J. Geophys. Res.*, *100*, 7865–7871, doi:10.1029/94JA03070.
Florinski, V., G. P. Zank, and N. V. Pogorelov (2003), Galactic cosmic ray transport in the global heliosphere, *J. Geophys. Res.*, *108*, 1228, doi:10.1029/2002JA009695.
Gleeson, L. J., and W. I. Axford (1968), Solar modulation of galactic cosmic rays, *Astrophys. J.*, *154*, 1011, doi:10.1086/149822.
Goelzer, M. L., C. W. Smith, N. A. Schwadron, and K. G. McCracken (2013), An analysis of heliospheric magnetic field flux based on sunspot number from 1749 to today and prediction for the coming solar minimum, *J. Geophys. Res. Space Physics*, *118*, 7525–7531, doi:10.1002/2013JA019404.
ICRP (1991), 1990 Recommendations of the International Commission on Radiological Protection, ICRP Publ. 60, Ann. ICRP 21(1–3).
Jokipii, J. R., E. H. Levy, and W. B. Hubbard (1977), Effects of particle drift on cosmic-ray transport. I—General properties, application to solar modulation, *Astrophys. J.*, *213*, 861–868, doi:10.1086/155218.
Joyce, C. J., et al. (2013), Validation of PREDICCS using LRO/CRaTER observations during three major solar events in 2012, *Space Weather*, *11*, 350–360, doi:10.1002/swe.20059.
Joyce, C. J., et al. (2014), Radiation modeling in the Earth and Mars atmospheres using LRO/CRaTER with the EMMREM Module, *Space Weather*, *12*, 112–119, doi:10.1002/2013SW000997.
le Roux, J. A., G. P. Zank, and V. S. Ptuskin (1999), An evaluation of perpendicular diffusion models regarding cosmic ray modulation on the basis of a hydromagnetic description for solar wind turbulence, *J. Geophys. Res.*, *104*, 24,845–24,862, doi:10.1029/1999JA900318.
Manuel, R., S. E. S. Ferreira, M. S. Potgieter, R. D. Strauss, and N. E. Engelbrecht (2011), Time-dependent cosmic ray modulation, *Adv. Space Res.*, *47*, 1529–1537, doi:10.1016/j.asr.2010.12.007.
McComas, D. J., R. W. Ebert, H. A. Elliott, B. E. Goldstein, J. T. Gosling, N. A. Schwadron, and R. M. Skoug (2008), Weaker solar wind from the polar coronal holes and the whole Sun, *Geophys. Res. Lett.*, *35*, L18103, doi:10.1029/2008GL034896.
McComas, D. J., N. Angold, H. A. Elliott, G. Livadiotis, N. A. Schwadron, R. M. Skoug, and C. W. Smith (2013), Weakest solar wind of the space age and the current "Mini" solar maximum, *Astrophys. J.*, *779*, 2, doi:10.1088/0004-637X/779/1/2.
McDonald, F. B., and L. F. Burlaga (1997), Global merged interaction regions, in *Cosmic Winds and the Heliosphere*, edited by J. R. Jokipii, C. P. Sonett, and M. S. Giampapa, pp. 581–616, Univ. of Ariz. Press, Tucson.
Mewaldt, R. A., A. J. Davis, W. R. Binns, G. A. de Nolfo, J. S. George, M. H. Israel, R. A. Leske, E. C. Stone, M. E. Wiedenbeck, and T. T. von Rosenvinge (2005), The cosmic ray radiation dose in interplanetary space present day and worst-case evaluations, *Proc. 29th Int. Cosmic Ray Conf.*, *2*, 433–436.
Mewaldt, R. A., et al. (2010), Record-setting cosmic-ray intensities in 2009 and 2010, *Astrophys. J. Lett.*, *723*, L1–L6, doi:10.1088/2041-8205/723/1/L1.
NASA (2007), NASA space flight human system standard volume. 1: Crew health, *Tech. Rep. NASA-STD-3001*, NASA Headquarters, Washington, D. C.
National Council on Radiation Protection and Measurements (NCRP) (1993), Limitation of exposure to ionizing radiation, *Tech. Rep. NCRP Rep. 116*, Natl. Counc. on Radiat. Prot. and Meas., Bethesda, Md.
National Council on Radiation Protection and Measurements (NCRP) (2000), Radiation protection guidance for activities in low-Earth orbit, *NCRP Tech. Rep. 132*, Natl. Counc. on Radiat. Prot. and Meas., Bethesda, Md.
Nealy, J. E., F. A. Cucinotta, J. W. Wilson, F. F. Badavi, N. Zapp, E. Semones, S. A. Walker, G. de Angelis, and S. R. Blattnig (2006), Pre-engineering spaceflight validation of environmental models and the 2005 HZETRN simulation code, paper presented by 36th COSPAR Scientific Assembly, COSPAR Meeting, Beijing, China.
Newkirk, G., Jr., A. J. Hundhausen, and V. Pizzo (1981), Solar cycle modulation of galactic cosmic rays: Speculation on the role of coronal transients, *J. Geophys. Res.*, *86*, 5387–5396, doi:10.1029/JA086iA07p05387.
NRC (2008), *Managing Space Radiation Risk in the New Era of Space Exploration*, Natl. Acad. Press, Washington, D. C.
NRC (2012), *Technical Evaluation of the NASA Model for Cancer Risk to Astronauts due to Space Radiation*, Natl. Acad. Press, Washington, D. C.
O'Neill, P. M. (2006), Badhwar O'Neill galactic cosmic ray model update based on Advanced Composition Explorer (ACE) energy spectra from 1997 to present, *Adv. Space Res.*, *37*, 1727–1733, doi:10.1016/j.asr.2005.02.001.
Owens, M. J., and N. U. Crooker (2006), Coronal mass ejections and magnetic flux buildup in the heliosphere, *J. Geophys. Res.*, *111*, A10104, doi:10.1029/2006JA011641.
Owens, M. J., N. A. Schwadron, N. U. Crooker, W. J. Hughes, and H. E. Spence (2007), Role of coronal mass ejections in the heliospheric hale cycle, *Geophys. Res. Lett.*, *34*, L06104, doi:10.1029/2006GL028795.
Potgieter, M. S., and J. A. Le Roux (1992), The simulated features of heliospheric cosmic-ray modulation with a time-dependent drift model: I. General effects of the changing neutral sheet over the period 1985–1990, *Astrophys. J.*, *386*, 336–346, doi:10.1086/171020.

Scherer, K., H. Fichtner, R. D. Strauss, S. E. S. Ferreira, M. S. Potgieter, and H.-J. Fahr (2011), On cosmic ray modulation beyond the heliopause: Where is the modulation boundary?, *Astrophys. J.*, *735*, 128, doi:10.1088/0004-637X/735/2/128.

Schwadron, N. (2012), Near-real-time situational awareness of space radiation hazards, *Space Weather*, *10*, 10005, doi:10.1029/2012SW000860.

Schwadron, N. A., and D. J. McComas (2008), The solar wind power from magnetic flux, *Astrophys. J. Lett.*, *686*, L33–L36, doi:10.1086/592877.

Schwadron, N. A., M. Owens, and N. U. Crooker (2008), The heliospheric magnetic field over the hale cycle, *Astrophys. Space Sci. Trans.*, *4*, 19–26, doi:10.5194/astra-4-19-2008.

Schwadron, N. A., A. J. Boyd, K. Kozarev, M. Golightly, H. Spence, L. W. Townsend, and M. Owens (2010a), Galactic cosmic ray radiation hazard in the unusual extended solar minimum between solar cycles 23 and 24, *Space Weather*, *8*, S00E04, doi:10.1029/2010SW000567.

Schwadron, N. A., et al. (2010a), Earth-Moon-Mars radiation environment module framework, *Space Weather*, *8*, S00E02, doi:10.1029/2009SW000523.

Schwadron, N. A., D. E. Connick, and C. Smith (2010b), Magnetic flux balance in the heliosphere, *Astrophys. J. Lett.*, *722*, L132–L136, doi:10.1088/2041-8205/722/2/L132.

Schwadron, N. A., C. W. Smith, H. E. Spence, J. C. Kasper, K. Korreck, M. L. Stevens, B. A. Maruca, K. K. Kiefer, S. T. Lepri, and D. McComas (2011), Coronal electron temperature from the solar wind scaling law throughout the space age, *Astrophys. J.*, *739*, 9, doi:10.1088/0004-637X/739/1/9.

Schwadron, N. A., et al. (2012), Lunar radiation environment and space weathering from the Cosmic Ray Telescope for the Effects of Radiation (CRaTER), *J. Geophys. Res.*, *117*, E00H13, doi:10.1029/2011JE003978.

Schwadron, N. A., M. L. Goelzer, C. W. Smith, J. C. Kasper, K. Korreck, R. J. Leamon, S. T. Lepri, B. A. Maruca, D. McComas, and M. L. Steven (2014), Coronal electron temperature in the protracted solar minimum, the cycle 24 mini maximum, and over centuries, *J. Geophys. Res. Space Physics*, *119*, 1486–1492, doi:10.1002/2013JA019397.

Shinn, J. L., J. W. Wilson, M. Weyland, and F. A. Cucinotta (1991), Improvements in computational accuracy of BRYNTRN (A Baryon transport code), *NASA Tech. Rep. 3093*, NASA, Springfield, Va.

Slaba, T. C., S. R. Blattnig, and F. F. Badavi (2010), Faster and more accurate transport procedures for HZETRN, *J. Comput. Phys.*, *229*, 9397–9417, doi:10.1016/j.jcp.2010.09.010.

Smith, C. W., N. A. Schwadron, and C. E. DeForest (2013), Decline and recovery of the interplanetary magnetic field during the protracted solar minimum, *Astrophys. J.*, *775*, 59, doi:10.1088/0004-637X/775/1/59.

Smith, C. W., K. G. McCracken, N. A. Schwadron, and M. L. Goelzer (2014), The heliospheric magnetic flux, solar wind proton flux, and cosmic ray intensity during the coming solar minimum, *Space Weather*, *12*, 499–507, doi:10.1002/2014SW001067.

Smith, E. J., and A. Balogh (2008), Decrease in heliospheric magnetic flux in this solar minimum: Recent Ulysses magnetic field observations, *Geophys. Res. Lett.*, *35*, L22103, doi:10.1029/2008GL035345.

Spence, H. E., et al. (2010), CRaTER: The Cosmic Ray Telescope for the Effects of Radiation experiment on the Lunar Reconnaissance Orbiter mission, *Space Sci. Rev.*, *150*, 243–284, doi:10.1007/s11214-009-9584-8.

Spence, H. E., M. J. Golightly, C. J. Joyce, M. D. Looper, N. A. Schwadron, S. S. Smith, L. W. Townsend, J. Wilson, and C. Zeitlin (2013), Relative contributions of galactic cosmic rays and lunar proton "albedo" to dose and dose rates near the Moon, *Space Weather*, *11*, 643–650, doi:10.1002/2013SW000995.

Stone, E. C., et al. (1998), The cosmic-ray isotope spectrometer for the advanced composition explorer, *Space Sci. Rev.*, *86*, 285–356, doi:10.1023/A:1005075813033.

Townsend, L. W., M. PourArsalan, F. A. Cucinotta, M. Y. Kim, and N. A. Schwadron (2011), Transmission of galactic cosmic rays through Mars atmosphere, *Space Weather*, *9*, S00E11, doi:10.1029/2009SW000564.

Wibberenz, G., I. G. Richardson, and H. V. Cane (2002), A simple concept for modeling cosmic ray modulation in the inner heliosphere during solar cycles 20–23, *J. Geophys. Res.*, *107*, 1353, doi:10.1029/2002JA009461.

Wilson, J. W., and F. F. Badavi (1986), Methods of galactic heavy ion transport, *Radiat. Res.*, *108*, 231-237.

Wilson, J. W., L. W. Townsend, W. S. Schimmerling, G. S. Khandelwal, F. S. Khan, J. E. Nealy, F. A. Cucinotta, L. C. Simonsen, J. L. Shinn, and J. W. Norbury (1991), Transport methods and interactions for space radiations, *NASA Tech. Rep. 1991-1257*, National Technical Information Service, Springfield, Va.

Wilson, J. W., J. E. Nealy, G. de Angelis, M. S. Clowdsley, and F. F. Badavi (2003), Deep space environment and shielding, in *Space Technology and Applications International Forum—STAIF 2003, Am. Inst. Phys. Conf. Ser.,* vol. 654, edited by M. S. El-Genk, pp. 993–1010, Albuquerque, N. M., doi:10.1063/1.1541395.

Zeitlin, C., et al. (2013), Measurements of energetic particle radiation in transit to Mars on the Mars Science Laboratory, *Science*, *340*(6136), 1080–1084, doi:10.1126/science.1235989.